doi:10.11835/j.issn.1671-8224.2018.01.02

To cite this article: LIAO Bang-liang, MA Jian-guang, ZHU Wei-hua, ZHU Hong-mei, YANG Kai, LIU Yan-hong, Li Huai-lin, WANG Xiao-jing, WANG Xin-lin. Microstructure and corrosion resistance of sputtered TiN coatings on surface of Zr-4 alloy [J]. J Chongqing Univ Eng Ed [ISSN 1671-8224], 2018, 17(1): 17-26.

Microstructure and corrosion resistance of sputtered TiN coatings on surface of Zr-4 alloy *

LIAO Bang-liang [1,†], MA Jian-guang [1], ZHU Wei-hua [2], ZHU Hong-mei [1], YANG Kai [1], LIU Yan-hong [3], LI Huai-lin [3], WANG Xiao-jing [3], WANG Xin-lin [1,2,‡,]

[1] *School of Mechanical Engineering, University of South China, Hengyang 421001, P. R. China*

[2] *School of Electrical Engineering, University of South China, Hengyang 421001, P. R. China*

[3] *State Power Investment Corporation Science and Technology Research Institute, Beijing 102209, P. R. China*

Received 17 October 2017; received in revised form 1 December 2017

Abstract: To improve the oxidation resistance and corrosion resistance of Zr-4 alloy, titanium nitride (TiN) coatings were prepared on the Zr-4 alloy with a TiN ceramic target with different ratios of N_2. Microstructure and high-temperature properties of the TiN coated samples were studied by scanning electron microscopy (SEM), energy dispersive spectrometer (EDS), X-ray diffraction meter (XRD), X-ray photoelectron spectroscopy (XPS), heat treatment furnace and autoclaves, respectively. The *x* value of the TiN coatings (TiN_x) ranges from 0.96 to 1.33. After the introduction of N_2, TiN coating exhibits a weak (200) plane and a preferred (111) orientation. The coating prepared with an N_2 flow ratio of 15% shows an optimal oxidation resistance in the atmospheric environment at 800 °C. In either 1 200 °C steam environment for one hour, or deionized water at 360 °C and a pressure of 18.6 Mpa for 16 d, the opitimized TiN coated samples have no delamination or spallation; and the gains in the masses of samples are much smaller than Zr-4 alloy. These results demonstrate the effectiveness of the optimized TiN coating as the protective coating on the Zr-4 alloy under extreme conditons.

Keywords: Zr-4 alloy; magnetron sputtering; TiN coating; high temperature oxidation resistance; corrosion resistance

CLC number: TH142 Document code: A

1 Introduction

Zirconium alloys have been widely used for fuel cladding tubes and other core components in nuclear reactors due to their low thermal neutron absorption cross-section, high fuel compatibility and excellent mechanical properties [1-2]. However, at a high temperature and high pressure in a nuclear reactor, zirconium alloy often suffers damages, such as frictional abrasion, neutron irradiation and hydrogen-absorption corrosion. These damages can cause failures of zirconium alloy as

† LIAO Bang-liang (廖帮亮): Bangliang_Liao@163.com.

‡ Corresponding author, WANG Xin-lin (王新林): wxl_ly000@aliyun.com.

* Funded by the National Science and Technology Major Project of the Ministry of Science and Technology of China (2015ZX06004001 -002) and the Postgraduate Research and Innovation Project of the University of South China (2017XCX11).

the protective nuclear fuel cladding tube [3-6]. To delay the failure of zirconium alloy, coatings usually are deposited on the surface of zirconium alloy by the coating deposition technology [7-9]. Thus, the coating deposition technology is an effective way to improve the physical and chemical properties of zirconium alloy and prolong its service life.

Among many coating deposition techniques, physical vapor deposition (PVD) methods are the popular technique, such as pulsed laser deposition [10], cathodic arc ion-plating [11] and magnetron sputtering [12]. Pulsed laser deposition can produce refractory films, and also can achieve the coincident ingredients between the film and the target [13]. But it is difficult to prepare the large area film, and the uniformity of the film is poor [14]. Cathodic arc ion-plating has the advantages of high deposition rate and high adhesion to the substrate [15]. Nevertheless, there are many micrometric and submicron particles on the surface of coatings prepared by cathodic arc ion-plating, which break the continuity of the membrane. In addition, in the process of cathodic arc ion-plating, the target is easy to be poisoned [16]. Compared with pulsed laser deposition and cathodic arc ion-plating, magnetron sputtering can decrease the poisoning degree of the target [17-19], and the coatings prepared by magnetron sputtering show a better surface quality [20-21]. Since the techniques of pulsed laser deposition and cathodic arc ion-plating have been used for preparing titanium nitride (TiN) coatings on the surface of zirconium alloy, and TiN coatings have excellent oxidation resistance and corrosion resistant properties [7-9]. Hence, TiN coatings by magnetron sputtering on the surface of Zr-4 alloy are worth studying.

In this work, by using magnetron sputtering, different TiN coatings were prepared on the surface of Zr-4 alloys by using a TiN ceramic target in a pure Ar atmosphere and an N_2/Ar mixed atmosphere, respectively. In the reactive magnetron sputtering process, TiN coatings were deposited with a little N_2. The features of TiN coatings including surface morphology, crystallographic properties, element content, stoichiometry of N/Ti, and high temperature oxidation were studied. After oxidation, the corrosion resistance of the optimized TiN coating with a superior oxidation resistance was investigated. The optimized TiN coating can be used as the protective coating on the Zr-4 alloy under extreme conditions.

2 Experimental

TiN coatings were deposited with a high purity TiN target (99.99% purity) in a pure Ar (99.99% purity) atmosphere and an N_2/Ar mixed atmosphere by d.c. (direct-current) magnetron sputtering, respectively. The flows of N_2 and Ar were regulated by two different mass flow controllers, respectively. The diameter of the target was 7.62 cm (3 inches). The X-ray diffraction (XRD) pattern of the target is shown in Fig. 1. The substrate was Zr-4 alloy with dimensions of 20 mm×20 mm×5 mm. Before deposition, Zr-4 alloys were burnished, mechanically polished, ultrasonically cleaned in an acetone and alcohol solution, and then pre-sputtered in a pure Ar atmosphere with a negative bias of 800 V for 10 min. During deposition, the substrate temperature was kept constant at 300 °C, and the working time was 180 min.

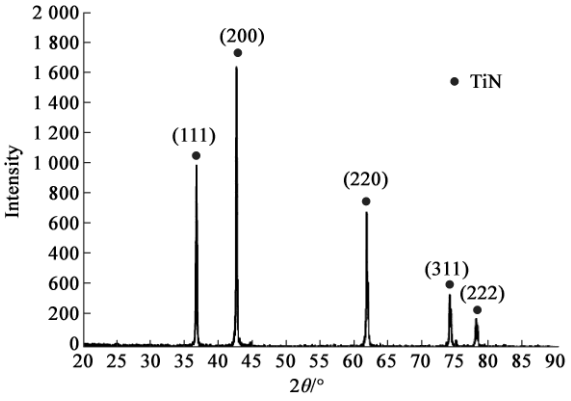

Fig. 1 XRD pattern of the TiN ceramic target

The total pressure was about 0.5 Pa. To perform the sputtering process in a nitrogen rich environment, the flow rate of Ar was maintained at 40 cm^3/min, and the flow rate of N_2 ranged from 0 to 10 cm^3/min. The specific synthesis conditions are summarized in Table 1.

Table 1 Parameters of the sputtering process

Sample No.	Power /W	Negative bias /V	N_2/%
1	300	–100	0
2	300	–100	7
3	300	–100	11
4	300	–100	15
5	300	–100	20

A type of XD-3 X-ray diffractometer equipped with a CuKα radiation source was used to investigate the phase structures of coatings, which was operated at 36 kV and 20 mA. The scanning speed was 2°/min, and the 2θ step was 0.02°. A JSM-6490LA scanning electron microscope (SEM) equipped with an energy dispersive spectrometer (EDS) was used to detect the surface morphology and element contents of coatings. To study the stoichiometry and the chemical binding state of the coatings, an axis ultra DLD type of X-ray photoelectron spectroscope (XPS) was used. The size of the mono-chromatized $Al_{K\alpha}$ source of X-ray beam was 700 μm×300 μm. The vacuum degree of analysis room was 0.67×10^{-6} Pa. High temperature oxidation resistance of the TiN coated samples was tested in the SX2-2.5 furnace. The mass gains of the oxidized samples were measured every 30 min on the BS210S electronic balance with a 0.01 g precision. The corrosion resistance of the optimized TiN coated samples was tested by a TGS-3B steam-heated autoclave and a YYF-50 static autoclave, and the samples were kept in the 1200 ℃ steam environment for 1 h and then in deionized water at 360 ℃ and 18.6 Mpa for 16 d, respectively.

3 Results and discussion

3.1 Surface morphology and microstructure

Small grains are observed in the surface morphology of TiN coatings with different ratios of N_2, as shown in Fig. 2. Coatings with N_2 ratios of 11% (Fig. 2c) and 15% (Fig. 2d) have fewer micro-particles and voids compared with those with N_2 ratios of 0% (Fig. 2a), 7% (Fig. 2b) and 20% (Fig. 2e). The surface morphology of the coating with an N_2 ratio of 15% (Fig. 2d) is the smoothest and densest. Fig. 3 shows the EDS patterns of coatings with different ratios of N_2; these coatings consist of elements Ti and N. Because nitrogen is the lighter element, the EDS is less sensitive to it. Thus, the intensities of element N of different coatings are all lower than those of element Ti, as shown in Fig. 3. In addition, the intensity of element Ti of the coating with an N_2 ratio of 15% (Fig. 3d) was the strongest. The deposition of TiN coatings by magnetron sputtering is a non-equilibrium process, and different N_2 flow ratios can have effects on the coating characteristics such as the surface morphology, chemical composition and phase [22]. When the migration rate of the particles is greater than the evaporation rate, the coating can grow constantly. When staying on the surface of the substrate, the particles only have surface diffusion energy and can find their thermodynamically stable positions before the single layer deposition is completed. Then these sputtered particles combine with each other to form larger atomic clusters on the surface of the substrate. Therefore, micro-particles and voids are often observed on the surface of the already formed continuous coating, and it is easy to generate dislocations at the edge of the holes due to the internal stress around the voids [10].

There usually exists a Ti or Ti_2N phase in the coatings by the reactive magnetron sputtering process from a Ti target in an N_2/Ar mixed atmosphere. Due to the high thermal neutron absorption cross-section of

the metal Ti, the ceramic target (TiN) is usually used as the sputtering target to avoid Ti phase in the TiN coatings. As can be seen obviously in Fig. 4, the coatings only have TiN and α-Zr phases. The α-Zr diffraction peaks are from the substrate. Compared with Fig. 1, TiN diffraction peaks appear to be broadened. After the addition of N_2, the TiN (200) plane is weakened, and the TiN (111) plane becomes the preferred orientation.

The preferred orientation of the coatings is important in application, which is always affected by magnetron sputtering process parameters, such as flow ratio of N_2, and negative bias. Because the TiN (200) plane has the lowest surface energy, and the TiN (111) plane has the minimum strain energy, the TiN preferred orientation depends on the competition between the surface free energy and the strain energy [23]. According to the research [24], coatings produced by physical gas phase deposition often have internal compressive stress on the level of (10^9 to 10^{10}) Pa. There also exists a significant shift toward the stress-free position in the angular position of the Zr diffraction peaks. With the addition of nitrogen molecules into TiN lattices, the TiN grain growth is restricted, the TiN grain boundaries increase, and the Ti lattices would distort within the nitrogen interstitial sites. The widened TiN peaks suggest a high degree of lattice distortion or grain refining of the TiN coating. Based on the Bragg equation [25]:

$$n\lambda = 2d\sin\theta, \tag{1}$$

where λ, d and θ are the X-ray wavelength, lattice space and diffration angle, respectively. The changes of θ angle can reflect the corresponding variation of the lattice parameter.

The TiN crystal has a type of NaCl structure, and the lattice parameter is 0.424 0 nm at stoichiometric composition [26]. Lattice constants calculated from TiN the (200) plane are shown in Table 2. According to the correlative equation [25]:

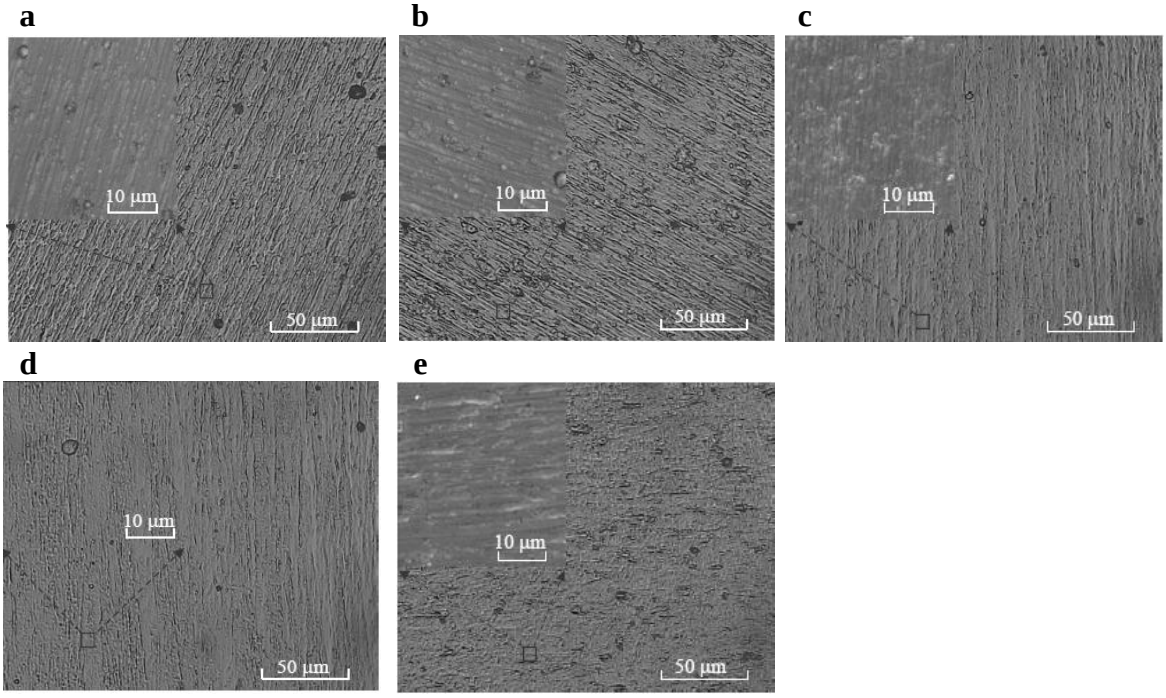

Fig. 2 Surface morphology recoded by the JSM-6490LA scanning electron microscope of the TiN coatings with different ratios of N_2: a) 0%; b) 7%; c) 11%; d) 15%; and e) 20%

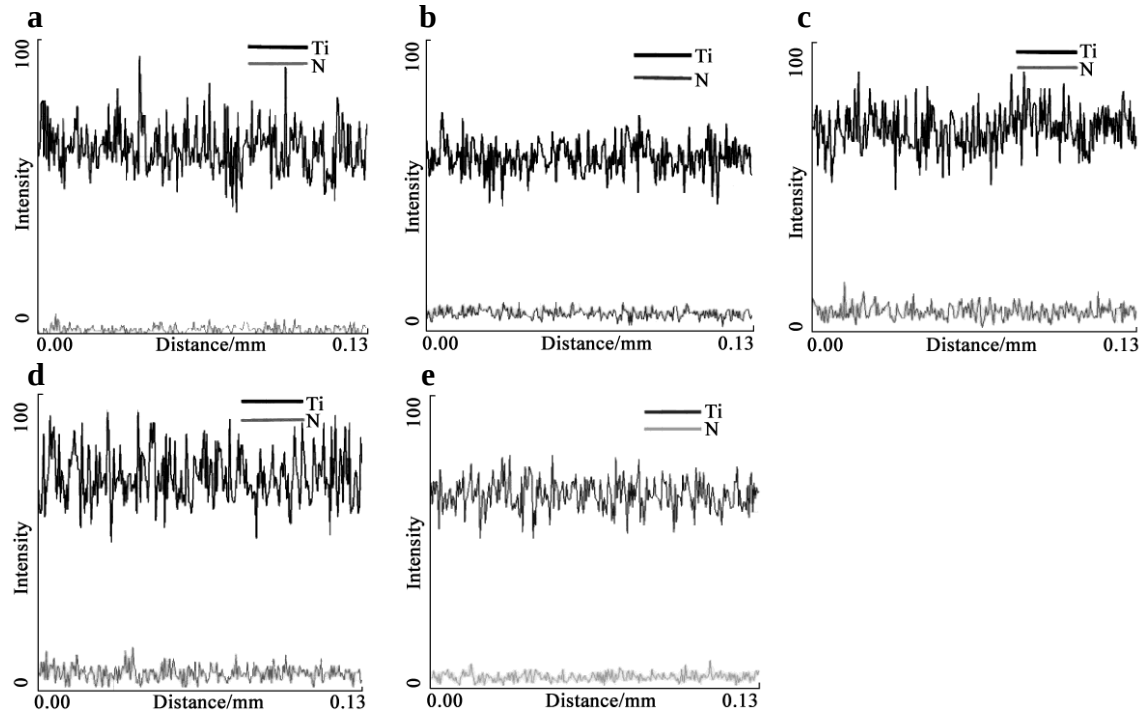

Fig. 3 EDS patterns of the TiN coatings with different ratios of N_2: a) 0%, b) 7%, c) 11%, d) 15%, and e) 20%

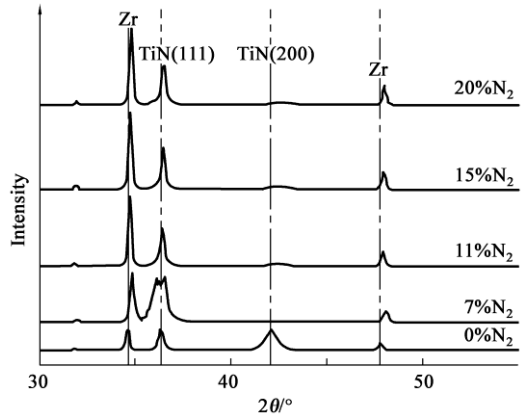

Fig. 4 XRD patterns of the TiN coatings with different ratios of N_2

$$a = d(h^2 + k^2 + l^2)^{1/2}, \quad (2)$$

where *h*, *k*, and *l* represent the indices of crystal faces.

Table 2 Lattice spacing (*d*) and lattice constant (*a*) of the TiN coatings

Sample No.	*d*/nm	*a*/nm
1	0.212 5	0.425 0
2	0.212 4	0.424 8
3	0.212 2	0.424 4
4	0.212 3	0.424 6
5	0.212 2	0.424 4

The lattice parameter of the coating ranges from 0.424 4 nm to 0.425 0 nm with the increase of nitrogen flow ratio from 0% to 20%. One reason for the lattice expansion phenomenon is the difference of the thermal expansion coefficients between the coating and the substrate, causing micro strain in the coating. Another reason can be the decrease of the average grain size.

Therefore, the lattice parameter can be regarded as a tool for identifying the structural disorder in the coatings.

3.2 Chemical binding states

The N/Ti ratios of the TiN coatings calculated from XPS data are shown in Fig. 5, which suggest the composition of stoichiometric and over-stoichiometric TiN_x coatings. After the reactive gas N_2 is introduced in the sputtering process, the TiN coating growth on the surface of Zr-4 alloy is in a nitrogen rich ambient. The composition of the gas phases can influence many parameters such as the sputtering yields, the nature of the extracted ions from the plasma, the secondary electron emission coefficients, and the composition of the coatings [27]. Nitrogen molecules from the gaseous phase can be physically adsorbed in the grain boundaries. Then nitrogen molecules and titanium atoms combine to form the over-stoichiometric TiN_x coatings. When the flow ratio of N_2 reaches 20%, the molecules of nitrogen in the chamber have reached a super-saturation state, and the collisions of sputtering particles and nitrogen molecules increase significantly. Therefore, the increased collision scattering phenomenon results in the decrease of the energy of the particles and gas molecules [28].

Fig. 6 shows the chemical binding states of TiN coatings. Due to the spin-orbit coupling effect, the Ti 2p energy level is divided into the stages of Ti $2p_{3/2}$ and Ti $2p_{1/2}$, which exhibits a bimodal structure in the XPS narrow-peak spectra. Generally, the area changes of XPS narrow-peak spectra, to a certain degree, reflect the variations of the element content, and the main contribution to the relative areas comes from the heights of the peaks [29]. With the increase of N_2 flow ratio, the intensities of Ti $2p_{3/2}$ and Ti $2p_{1/2}$ peaks increase. When the N_2 flow ratio is 15%, the intensities of Ti $2p_{3/2}$ and Ti $2p_{1/2}$ peaks are the strongest, which is consistent with the results in Fig. 3d. The two peaks of Ti 2p energy level move toward the direction of lower binding energy constantly, which can be associated with the formation of TiN bonds and vacancies [30]. Furthermore, the variability of the valence state of Titanium and the tendency to vacancy formation in its compounds, in a nitrogen rich ambient, provides a large possibility for the formation of various stoichiometric and over-stoichiometric compounds or phases in TiN coatings [31-32].

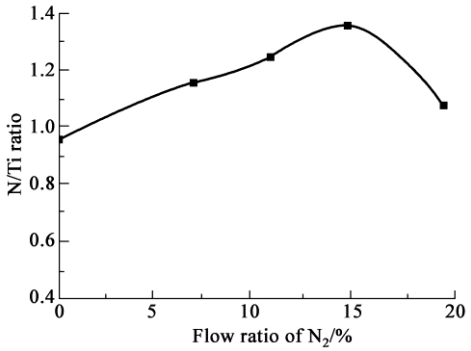

Fig. 5 Evolution of the N/Ti ratios versus different ratios of N_2 on the deposited TiN coatings

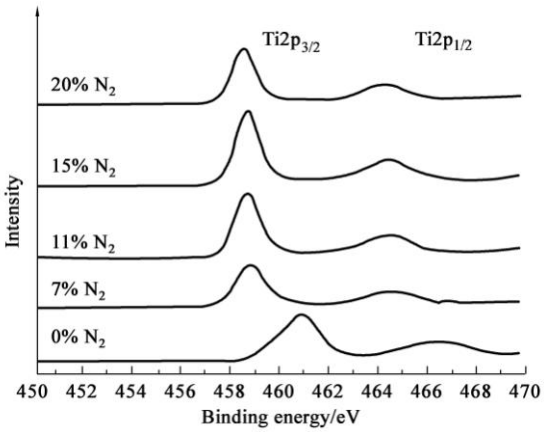

Fig. 6 X-ray photoelectron spectra of Ti 2p for the TiN coatings with different ratios of N_2

3.3 High temperature oxidation and corrosion resistance

Fig. 7 shows the mass gains of Zr-4 alloy and TiN

coated samples over time at 800 °C. Before 120 min, the mass gains of the TiN coatings increase slowly. After 120 min, the mass gains of the TiN coatings increase quickly. In the whole oxidization process, the mass gain of Sample 4 is the smallest, and there is no cracking and no debonding by visual examination. However, the high temperature oxidation properties of TiN coatings critically depend on the actual composition, structure and chemical binding state. Due to Samples 1 and 2 having many defects (as seen in Fig. 2), the mass gains of Samples 1 and 2 are higher than other TiN coated samples. According to the intensities of element Ti and the stoichiometry of N/Ti (as seen in Fig. 3d and Fig. 6), Samples 3 and 4 possess more saturated Ti-N bonds than other TiN coated samples, which results in Samples 3 and 4 having a smaller mass gain under a high temperature oxidation condition. When the ratio of N_2 reaches 20%, the collision scattering phenomenon occurs, causing the decrease of the energy of the particles and gas molecules, and increase of the porosity of the coating [28]. Therefore, the mass gain of Sample 5 is larger than that of Sample 4.

Due to the superb oxidation resistance properties of Sample 4 in an atmospheric environment at 800 °C, Sample 4 was chosen to evaluate the out-of-pile corrosion test in 1 200 °C steam environment and at 360 °C and 18.6 Mpa conditions. Zr-4 alloy was also tested under the same conditions for a comparison.

As shown in Table 3, the mass gain of the TiN coated sample (4.318 5 g/dm^2) in the 1 200 °C steam environment for 1 h is lower than that of Zr-4 alloy (4.572 0 g/dm^2) and the standard line (3.538 98 to 4.325 42) g/dm^2), and there is no spallation or delamination on the surface of the TiN coated sample. The result shows that TiN coating has a protective effect for Zr-4 alloy under a high temperature oxidation condition. As seen from Table 4, the mass gain (0.16 mg) and the mass gain ratio (0.001 27%) of Sample 4 in a static autoclave of 360 °C deionized water at 18.6 Mpa for 16 d are much lower than those of Zr-4 alloy, and the TiN coated sample is not subject to shedding or debonding phenomenon, which is consistent with the findings of other related research [8-9]. Thus, the optimized TiN coating depositing on the surface of Zr-4 alloy shows a good adhesion to the substrate and has a better oxidation and corrosion resistance in high temperature and high pressure conditions.

4 Conclusions

1) TiN_x coatings with an x value from 0.96 to 1.33 were prepared in this work. After the introduction of N_2, the TiN coatings exhibited a weak (200) plane and a preferred (111) plane.

2) With the increase of N_2 ratio, Ti 2p moves toward the lower binding energy direction constantly, which can be associated with the formation of TiN bonds and vacancies.

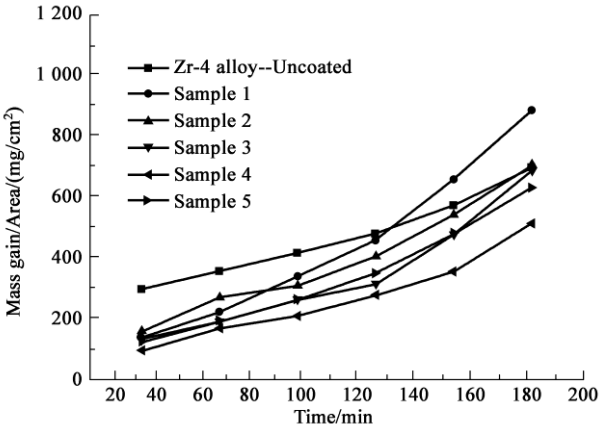

Fig. 7 Mass gains in the atmospheric environment at 800 °C of uncoated Zr-4 alloy, and TiN coated samples of different N_2 ratios: Sample 1. 0%, Sample 2. 7%; Sample 3. 11%; Sample 4. 15%, and Sample 5. 20%

Table 3 Zr-4 alloy and Sample 4 in 1 200 ℃ steam environment for 1 h

Specimen	Surface area /mm^2	Mass gain of 0.5 h /(g/dm^2)	Mass gain of 1.0 h /(g/dm^2)
CP1200 (standard line)	460	2.502 5 to 3.058 6	3.538 98 to 4.325 42
Zr-4 alloy	460	3.038 2	4.572 0
Sample 4	460	3.058 8	4.318 5

Table 4 Zr-4 alloy and Sample 4 at 360 ℃ and 18.6 Mpa for 16 d

Specimens	Original mass /g	Mass of 16 d /g	Mass gain/mg	Rate /%	Combining conditions
Zr alloy	12.644 44	12.644 92	0.48	0.003796	
Sample 4	12.601 44	12.601 60	0.16	0.001270	No shedding

3) The TiN-coated sample prepared with a 15% flow ratio of N_2 shows the optimal oxidation resistance without crack and spallation in an atmospheric environment at 800 ℃, and the TiN coating can withstand the steam environment at 1 200 ℃ for 1 h and a static autoclave of deionized water at 360 ℃ and 18.6 Mpa for 16 d. The optimized TiN coating is of a excellent adhesion to the Zr-4 alloy substrate.

4) Combined with the physical properties of the TiN coating, it is found that the optimized TiN coating could be used as the protective layer for the improvement of oxidation resistance and corrosion resistance of Zr-4 alloy.

Acknowledgements

This work was supported by the National Science and Technology Major Project of the Ministry of Science and Technology of China (2015ZX06004001-002) and the Postgraduate Research and Innovation Project of the University of South China (2017XCX11).

References

[1] PENG D Q, BAI X D, PAN F, et al. Influence of aluminum ions implanted on oxidation behavior of ZIRLO alloy at 500 ℃ [J]. Vacuum, 2006, 80(6): 530-536.

[2] CLEMENT L, MOTTA A T. Zirconium alloys in nuclear applications [M]. Weinheim: Wiley-VCH Verlag GmbH & Co. KGaA, 2006.

[3] KIM H K, LEE Y H, HEO S P. Mechanical and experimental investigation on nuclear fuel fretting [J]. Tribology International, 2006, 39(10): 1305-1319.

[4] LEE S J, PARK C J, LIM Y S, et al. Influences of laser surface alloying with niobium (Nb) on the corrosion resistance of Zircaloy-4 [J]. Journal of Nuclear Materials, 2003, 321(2): 177-183.

[5] ZINKLE S J, TERRANI K A, GEHIN J C, et al. Accident tolerant fuels for LWRs: a perspective [J]. Journal of Nuclear Materials, 2014, 448(1/2/3): 374-379.

[6] KIM H G, YANG J H, KIM W J, et al. Development

status of accident-tolerant fuel for light water reactors in Korea [J]. Nuclear Engineering & Technology, 2016, 48(1): 1-15.

[7] KHATKHATAY F, JIAO L, JIAN J, et al. Superior corrosion resistance properties of TiN-based coatings on Zircaloy tubes in supercritical water [J]. Journal of Nuclear Materials, 2014, 451(1/2/3): 346-351.

[8] ALAT E, MOTTA A T, COMSTOCK R J, et al. Ceramic coating for corrosion (c3) resistance of nuclear fuel cladding [J]. Surface & Coatings Technology, 2015, 281: 133-143.

[9] ALAT E, MOTTA A T, COMSTOCK R J, et al. Multilayer (TiN, TiAlN) ceramic coatings for nuclear fuel cladding [J]. Journal of Nuclear Materials, 2016, 478: 236-244.

[10] KIM I, KHATKHATAY F, JIAO L, et al. TiN-based coatings on fuel cladding tubes for advanced nuclear reactors [J]. Journal of Nuclear Materials, 2012, 429(1/2/3): 143-148.

[11] BALASHABADI P, LARIJANI M M, SHOKRI A A, et al. The effect of bias voltage on microstructure and hardness of TiN films grown by ion coating deposition [J]. European Physical Journal Plus, 2015, 130(2): 1-10.

[12] JIANG F, ZHANG T F, WU B H, et al. Structure, mechanical and corrosion properties of TiN films deposited on stainless steel substrates with different inclination angles by DCMS and HPPMS [J]. Surface & Coatings Technology, 2016, 292: 54-62.

[13] ZHERIKHIN A N. Pulsed laser deposition of thin films [J]. Proceedings of SPIE - The International Society for Optical Engineering, 1999, 3571(7): 72-79.

[14] STOYANOV D V. Pulsed laser deposition of thin films [M]. [S.l.]: Wiley, 1994: 648.

[15] YAO X H, TANG B, TIAN L H, et al. Microstructure and corrosion resistance of TiN coating on HSS by pulsed bias cathodic arc ion plating [J]. Materials Science Forum, 2011, 675-677: 1307-1310.

[16] TAKIKAWA H, TANOUE H. Review of cathodic arc deposition for preparing droplet-free thin films [J]. IEEE Transactions on Plasma Science, 2007, 35(4): 992-999.

[17] MAYRHOFER P H, KUNC F, MUSIL J, et al. A comparative study on reactive and non-reactive unbalanced magnetron sputter deposition of TiN coatings [J]. Thin Solid Coatings, 2002, 415(1): 151-159.

[18] KAWAMURA M, KUMAGAI K, ABE Y, et al. Characterization of TiN films prepared by r.f. sputtering using metal and compound targets [J]. Vacuum, 1998, 51(3): 377-380.

[19] MARTINEZ-MARTINEZ D, LOPEZ-CARTES C, FERNANDEZ A, et al. Exploring the benefits of depositing hard TiN thin coatings by non-reactive magnetron sputtering [J]. Applied Surface Science, 2013, 275(21): 121-126.

[20] 白秀琴,李健.低温磁控溅射与普通多弧离子镀TiN薄膜的摩擦学性能比较[J].中国表面工程,2006,19(1): 12-15.
BAI X Q, LI J. A comparison of the tribological properties between low temperature magnetic sputtering and multi-arc ion plating TiN films [J]. China Surface Engineering, 2006, 19 (1): 12-15. (In Chinese).

[21] 李鹏,黄美东,佟莉娜,等.磁控溅射与电弧离子镀制备TiN薄膜的比较[J].天津师范大学学报(自然版),2011, 31(2):32-37.
LI P, HUANG M D, TONG L N, et al. Comparison of TiN films prepared by magnetron sputtering and arc ion plating [J]. Journal of Tianjin Normal University (Natural Edition), 2011, 31(2): 32-37. In Chinese).

[22] ZEMAN P, TAKABAYASHI S. Nano-scaled photocatalytic TiO_2 thin films prepared by magnetron sputtering [J]. Thin Solid Films, 2003, 433(1/2): 57-62.

[23] LI T Q, NODA S, TSUJI Y, et al. Initial growth and texture formation during reactive magnetron sputtering of TiN on Si(111) [J]. Journal of Vacuum Science & Technology, 2002, 20(3): 583-588.

[24] SOLOVEV A A, SOCHUGOV N S, OSKOMOV K V. Effect of residual internal stresses in TiN coatings on specific losses in anisotropic electrical steel [J].

Physics of Metals & Metallography, 2010, 109(2): 111-119.

[25] POPE C G. X-ray diffraction and the bragg equation [J]. Journal of Chemical Education, 1997, 74(1): 129-131.

[26] TOTH L E. Transition metal carbides and nitrides [M]. New York: Academic Press, 1971.

[27] BRETAGNE J, BOISSE LAPORTE C, GOUSSET G, et al. Fundamental aspects in non-reactive and reactive magnetron discharges [J]. Plasma Sources Science & Technology, 2003, 12(4): S33.

[28] COMBADIERE L, MACHET J. Study and control of both target-poisoning mechanisms and reactive phenomenon in reactive planar magnetron cathodic sputtering of TiN [J]. Surface & Coatings Technology, 1996,82(1/2): 145-157.

[29] BENDER H, PORTILLO J, VANDERVORST W. Quantitative AES and XPS investigation of magnetron sputtered TiNx films [J]. Surface & Interface Analysis, 1989, 14(6/7): 337-346.

[30] ERMOLIEFF A, BERNARD P, MARTHON S, et al. Nitridation of polycrystalline titanium as studied by in situ angle-resolved x-ray photoelectron spectroscopy [J]. Surface & Interface Analysis, 2010, 11(11):563-568.

[31] MURRAY J L. Phase diagrams of binary titanium alloys [M]. Ohio: ASM International, 1987: 12-24.

[32] BERTOTI I, MOHAI M, Sullivan J L, et al. Surface characterisation of plasma-nitrided titanium: an XPS study [J]. Applied Surface Science, 1995, 84(4): 357-371.